Journal of Engineering Mathematics **31:** 285–303, 1997.

On the mechanics of the arrow: Archer's Paradox

B.W. KOOI *
Galvanistraat 14, 1433 MA Kudelstaart, The Netherlands

J.A. SPARENBERG
Department of Mathematics and Computer Science, University of Groningen, P.O. Box 800, 9700 AV Groningen, The Netherlands

Received 3 January 1995; accepted in revised form 11 March 1996

Abstract. In ancient bows the grip of the bow was in the way of the arrow. The arrow needed to get round the bow while being accelerated; this phenomenon is called the 'Archer's Paradox'. In the forties it was observed experimentally with high-speed cameras that the arrow vibrates in a horizontal plane perpendicular to the vertical median plane of the bow. These movements are started and controlled by the movements of the two points of contact with the bow, *viz.* the middle of the string in contact with the rear end of the arrow and the grip where the arrow slides along the bow. The latter contact imposes a moving-boundary condition. The numerically obtained results are satisfactorily in agreement with experimental data. The model can be used to estimate the drawing force of ancient bows of which only the contemporary arrows are available and also for the design of new archery equipment.

Key words: Archery, arrow motion, Archer's Paradox, finite-difference technique, moving-boundary problem

1. Introduction

One of the most fascinating phenomena in archery is called the 'Archer's Paradox'. We start with a simplified exposition of this seeming contradiction. The origin of the paradox is the vibration of the arrow in a horizontal plane after it has been released, while the bow is kept vertical. The vibration is caused by the bending of the arrow during and after its release. In principle, there are the following two different causes for this bending of the arrow.

The first is related to the way in which the arrow is released; here we are considering the Mediterranean release. When the bow is fully drawn, it is kept in this position by three fingers of the archer hooked on the string, the forefinger above and two fingers below the nock (grooved rear end) of the arrow. When the arrow is launched, the string slips off the three finger tips and in this way the nock of the arrow is moved swiftly sideways. Hence, by its inertia, the arrow will bend.

The second cause of the bending of the arrow is related to the width of the rigid middle part of the bow, called the grip or handle. When we consider a classical bow in fully drawn position, the arrow will form a small angle with the median plane of the bow. After release this angle increases swiftly, because the distance between nock and grip decreases swiftly. Then again by inertia the arrow will bend.

The bending resulting from the two mentioned causes is increased by the large longitudinal force exerted by the string on the nock. This force has a buckling effect on the arrow.

* address for correspondence: *Department of Biology, Free University, De Boelelaan 1087, 1081 HV Amsterdam, The Netherlands*

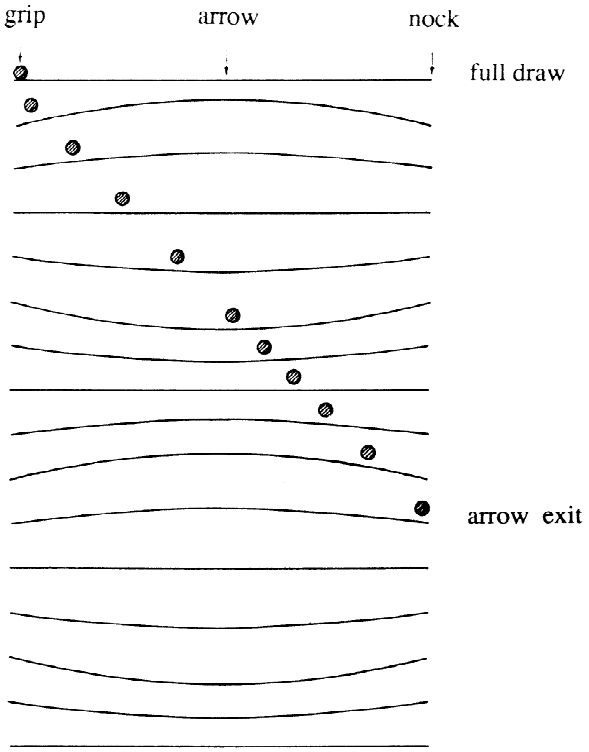

Figure 1. Illustration of Archer's Paradox (after Klopsteg [1, page 182]). Schematic representation of shapes of arrow during its passage of the bow, based on evidence from speed-flash photography.

The results of the two causes of the bending of the arrow can intensify each other or reduce each other. It is not difficult to see that they reduce each other, for the classical bow, when the arrow rests on the knuckle of the forefinger of the bow hand, *i.e.* the hand that grips the bow. Perhaps this is the reason that this way of shooting was and still is in use with classical bows.

When the arrow leaves the string it is still curved and starts to vibrate freely in a horizontal plane with a frequency which depends on its mass distribution and on its flexural rigidity distribution. Now the inertial and the elastic properties of the arrow have to be such that, while passing the grip of the bow, the arrow does not slap with its rear end against the grip but snakes around it, otherwise the accuracy of the shooting would be decreased. The phenomenon of the arrow snaking around the grip of the bow is called the Archer's Paradox. In Figure 1 the paradox is illustrated as taken from Klopsteg [1, page 182].

An application of the above-mentioned phenomenon can be made as follows. We assume that in former times, when the bow was an important weapon, the arrow was matched, possibly by trial and error, to a bow so that after release it could pass the grip without impediment. In that case there is a relation between the properties of the bow such as its draw length, its draw weight (force in fully drawn position) and the inertial and elastic properties of the arrow. This relation makes it possible to estimate the draw weight of a bow when arrows which have been shot from the bow are available.

Calculations suggested that the heavy 60 gram war arrows as used at Agincourt in 1415 during the Hundred-Years War, could have been shot from bows with a draw weight of over 450 N. This, however, seemed an unreasonably large value: nowadays only a few archers can master bows of such a great weight. Based on present-day experience a figure closer to

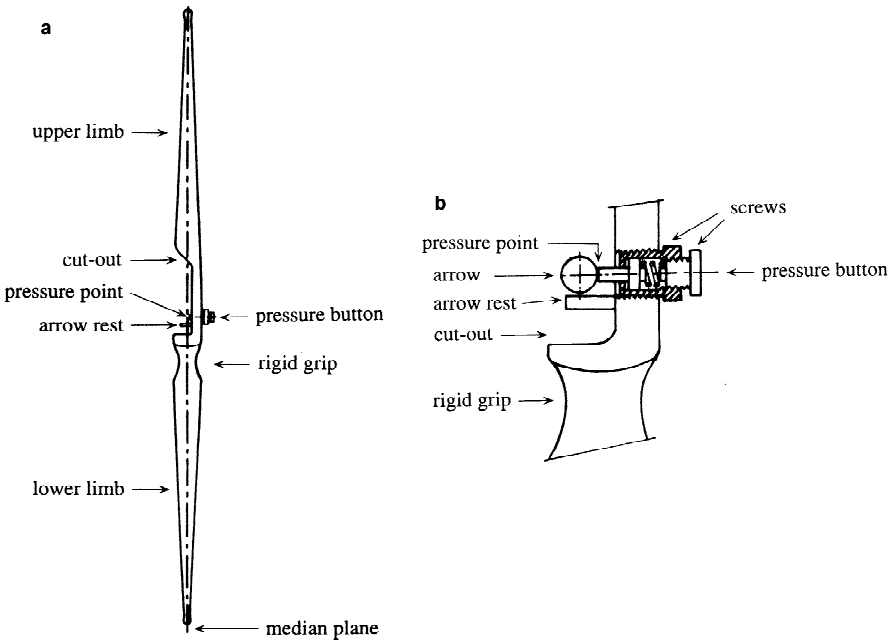

Figure 2. (a) Modern right-handed bow with cut-out. (b) Enlarged cross-section of grip with arrow rest and pressure point. The outer screw adjusts the whole pressure button mechanism in and out the median plane and the inner screw adjusts the initial compression of the spring.

350 N was thought more likely. The high value of over 450 N was, however, confirmed by the study of 139 longbows and over 3000 arrows recovered from the Mary Rose (Hardy [2] and Paterson [3]). The Mary Rose was a warship of Henry VIII, which sank in 1545 and was recovered in 1982. In [2] it is stated that: "young, fit men in constant practice chosen for well-paid military service from a nation to whom the shooting of longbows had been second nature", could use the heavy Mary-Rose bows.

Hickman invented the so-called centre-shot bow. A cut-out of the grip of the bow allows the arrow to move in the median plane of the bow in which the elastic limbs move (Figure 2a). When the bow string is drawn by the right hand (right-handed bow), the cut-out is at the left side of the bow as seen by the archer and inversely for the left-handed bow where the string is drawn by the left hand. The arrow is vertically supported by an arrow rest, a slender elastic projection on the side of the bow in the cut-out. The point of contact with the grip, where the lateral motion of the arrow is one-sidedly constrained, is called the pressure point. Nowadays a pressure button is often used for this constraint. This is a small spring-loaded rod with a piece of slippery plastic on the end (Figure 2b). The amount of protrusion of the pressure point out of the median plane of the bow, as well as the compression of the spring of the pressure button, can be separately adjusted by means of two screws.

Already in the forties Hickman [1] took high-speed pictures of the vibrating arrow and showed that the bending properties of the arrow are important. Also Pękalski [4, 5] showed by means of a high-speed film the shape of the vibrating motion of the arrow and gave a theoretical treatment of the snaking phenomenon.

To study the paradox, we have developed a mathematical model for the lateral movements of the arrow. For this reason we have needed the longitudinal force acting on the arrow, which follows from our previous work of which we give a short survey. We dealt with the dynamics of the bow and arrow, using a simple representation of the arrow, namely a point-mass placed at the middle of the string [6]. The elastic limbs of the bow were represented by elastic lines with a non-uniform mass distribution and a non-uniform flexural rigidity distribution, undergoing large deflections. For the quasi-static deformation of the bow from the braced situation (straight string) to the fully drawn situation, the equations for this geometrically nonlinear model were solved numerically by means of the repeated application of a mathematical "shooting" method [7]. This yields the Static-Force-Draw curve (SFD curve) which shows the force exerted by the archer when deforming the bow to full draw.

A finite-difference technique was used for the solution of the dynamic equations of the bow and arrow (point-mass) after release [8, 9]. This yields the Dynamic-Force-Draw (DFD) curve which gives the acceleration force exerted by the string on the arrow as a function of traveled distance. Both curves differ significantly from each other, which is caused by the inertia of the bow limbs as is explained in Section 2.

The mechanics of the "arrow", which is the subject of this paper, is treated partly uncoupled from the mechanics of the "bow and arrow". For the mechanics of the arrow we use, for the acceleration force exerted by the string on the nock of the arrow, the DFD curve mentioned in the previous paragraph. The arrow is now considered as a vibrating beam with two point-masses, namely the nock at the rear end and the arrowhead at the front end. The arrow slides without friction over the arrow rest by which it is supported vertically and along the pressure point by which it is unilaterally constrained horizontally. The swift transverse movement of the nock during release, caused by the slipping of the string from the finger tips, will be assumed to be known.

The transverse vibratory movement of the arrow is described by two systems of partial differential equations (PDE's) when the arrow has contact with the pressure point. Each system is valid on one of the two adjacent spatial intervals covering the arrow. The connection point of these intervals is at the pressure point. At this point the transverse displacement of the two intervals and some of their spatial derivatives have to satisfy suitable relations, as will be discussed in Section 2. The position of the pressure point varies with respect to the arrow, which renders the problem a moving-boundary problem. Because in our formulation the longitudinal acceleration of the arrow is known in advance, the place of the moving boundary is known with respect to the arrow. When the arrow has lost contact with the pressure point, only one system of PDE's is needed which is valid along the whole length of the arrow. Further there are in both cases two boundary conditions, one at the rear end being the equation of motion of the nock and another at the front end being the equation of motion of the arrowhead. Initial conditions complete the formulation of the problem.

Pękalski's mathematical model [4, 5] and his analysis was the incentive for reconsidering the problem. The model presented here is more accurate than Pękalski's model, due to less stringent assumptions. For instance the acceleration of the arrow and consequently the longitudinal buckling force caused by the acceleration is rather large and may not be neglected. Also, the release is modeled more realistically and this gives a better start for the bending of the arrow.

In Section 3 a finite-difference scheme is developed to solve the set of PDE's numerically. In Section 4 we compare our results with the theoretical results obtained by Pękalski and with the bending shapes of the arrow as obtained by his high-speed film. It appears that during the

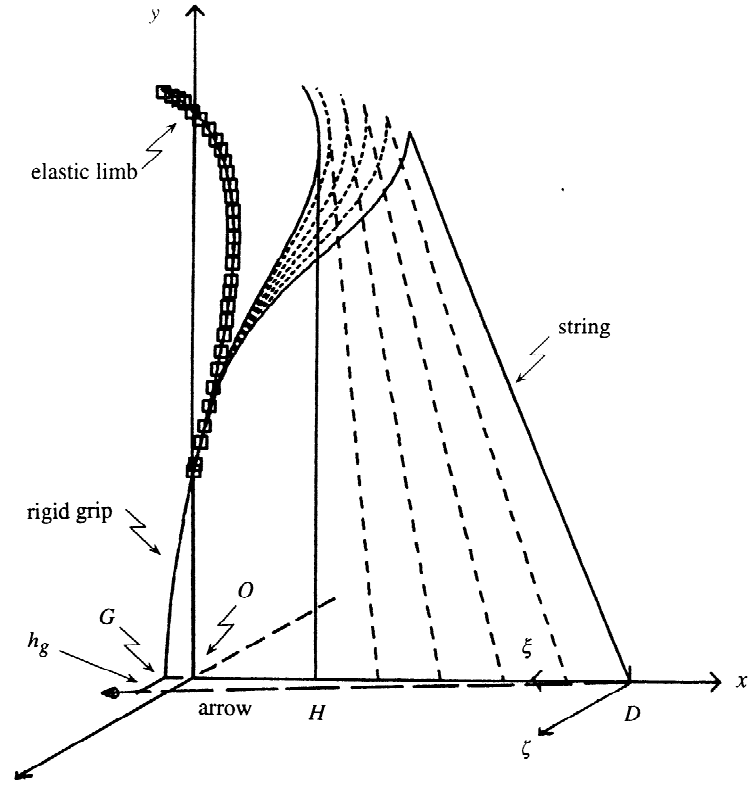

Figure 3. Static deformation of the modern working-recurve bow: the unbraced bow (□), braced bow and fully drawn bow (——) and some intermediate situations (– –). At $t = 0$ the arrow and the moving-coordinate system (ξ, ζ), in which the transverse movement of the arrow is described, are shown.

important last part of the period of time before the nock of the arrow passes the grip of the bow, our calculated shapes of the arrow are closer to reality than those of Pękalski.

2. Formulation of the problem

We start with a short, more systematic, description of the bow where possibly some repetitions occur of subjects mentioned in the introduction. The reader is referred to [6, 9], for instance, for an elaborate discussion. The braced bow (straight string) is placed in a right-handed Cartesian coordinate system (x, y, z), being an inertial frame of reference (see Figure 3). The x-axis coincides with the line of symmetry of the bow and the origin O is the intersection of this line with the line that connects the points where the rigid middle part of the bow meets the elastic limbs. The z-axis is perpendicular to the vertical median plane of the bow. When the bow is drawn quasi-statically from the braced situation to full draw, the x-coordinate of the middle of the string coincides with the nock of the arrow and is denoted by b.

In Figure 3 the unbraced, the braced ($b = |OH|$) and the fully drawn ($b = |OD|$) shapes of a modern working-recurve bow are schematically shown. The distance $|OH|$ is called the brace height and the distance $|OD|$ the draw. The static force exerted by the archer in the positive x-direction, is denoted by $F(b)$ which follows directly from the already mentioned SFD curve. In the fully drawn situation, the force $F(|OD|)$ is called the weight of the bow. The

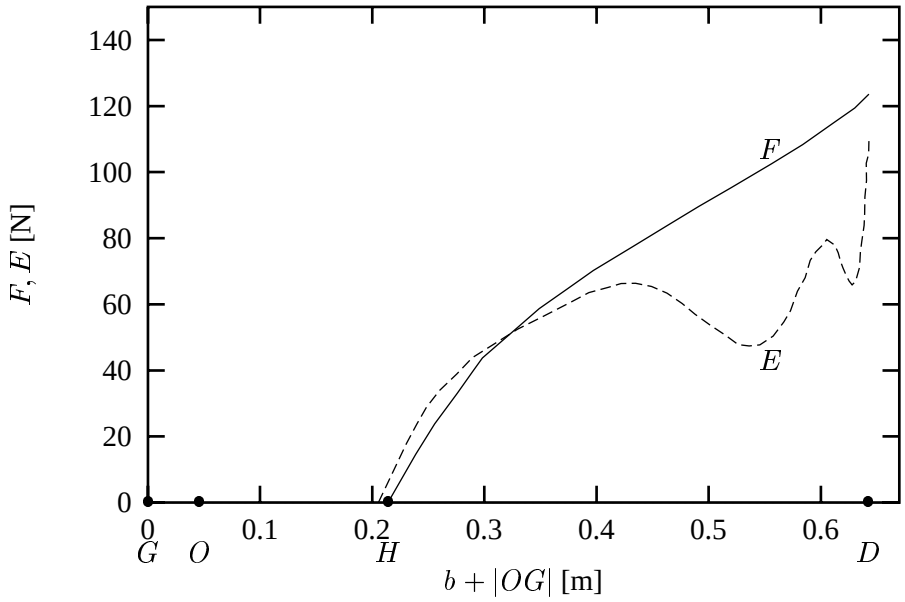

Figure 4. Calculated Static-Force-Draw curve, $F(b)$ (——), and Dynamic-Force-Draw curve, $E(b)$ (– –), of a modern working-recurve bow (Greenhorn Comet TD 350, 68 inch, 30 lbs).

projection of the pressure point on the x-axis is indicated by G, this is also the point where the archer holds the bow and which can be considered as the pivot point of bow rotations which can occur after release. The components of the distance between the origin and the pressure point in the x- and z-direction are denoted by $|OG|$ and h_g, respectively. For ancient bows $|OG| = 0$ and h_g is the half width of the grip. In Table 1 a survey of various parameters of a bow and arrow is given.

In Figure 4 we show, for a modern working-recurve bow as discussed in [9], the calculated SFD ($F(b)$) and the DFD ($E(b)$) curves, where $E(b)$ is the acceleration force acting upon the arrow as function of b. The mass of the rather stiff string is lumped into three mass points each equal to one-third of the mass of the string. These points are at the two tips of the limbs and in the middle of the string where it adds to the mass of the nock of the arrow. The addition of the lumped part of the mass to the nock is only used with respect to the calculation of the DFD curve and not later on with respect to transverse motions. At release ($t = 0+$) the acceleration force $E(|OD|)$, is smaller than the static draw-force, $F(|OD|)$. This remains true for some time. This is caused by the mass of the elastic limbs and the inertia of the added parts of the string, which have to be accelerated as well. After this period of time, $E(b)$ is larger than $F(b)$ because then the inertia of the limbs, which then are decelerated, adds to the force on the arrow. Arrow exit at $t = t_l$, when the arrow leaves the string, is defined by the instant the acceleration force $E(b)$ becomes zero.

The arrow is inextensible and its longitudinal motion is determined by the acceleration force $E(t) = E(b(t))$. Only transverse deflections which are small with respect to the length of the arrow will be considered. The arrow is placed in a moving Cartesian coordinate system (ξ, ζ), the ξ-axis coinciding with x-axis, but pointing in the opposite direction and the ζ-axis parallel to the z-axis. The origin of the (ξ, ζ) system has the same x-coordinate as the nock of the arrow (Figures 3 and 5).

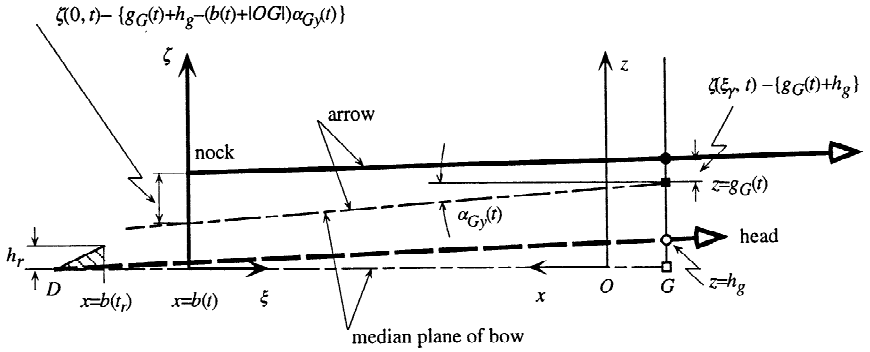

Figure 5. Coordinate system (ξ, ζ) in which transverse motion of arrow is described. Displacement and rotation of bow are $g_G(t)$ and $\alpha_{Gy}(t)$. Transverse displacement of nock, $\zeta(0,t)$, is sum of displacement caused by the movement of the bow, $g_G(t) + h_g - (b(t) + |OG|)\alpha_{Gy}(t)$, and elongation of spring which represents transverse elasticity of bow, see (8). (□) is position of pivot point G and (○) is position of pressure point, at $t = 0$. (■) and (●) represent positions for $t > 0$. During release nock slides along hypotenuse of hatched right-angled triangle.

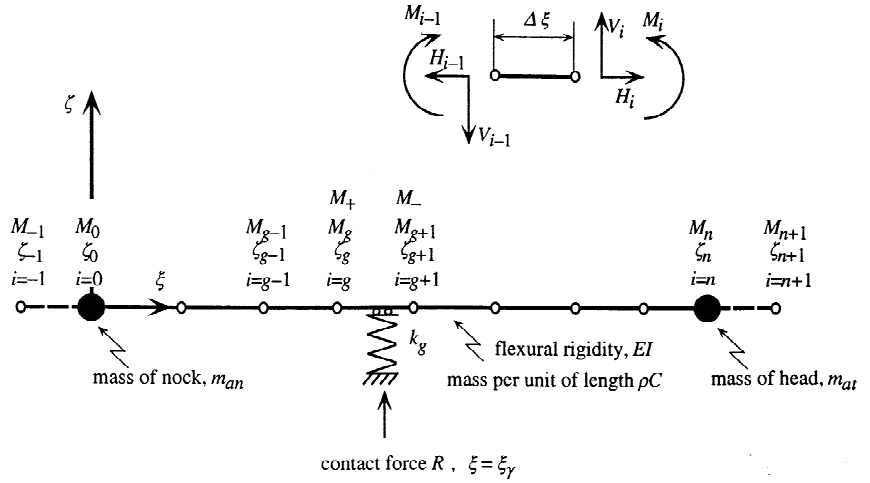

Figure 6. Scheme of model of arrow. Each element, $i = 1, \cdots, n$, has length $\Delta\xi$. Between grid-points we have mass per unit of length ρC and flexural rigidity EI. Two fictitious points outside arrow are introduced, grid-points $i = -1$ and $i = n + 1$. Pressure point at $\xi = \xi_\gamma$. Grid point to the left of pressure point is denoted by g. Two extra unknown bending moments M_- and M_+ at points g and $g + 1$, respectively.

The arrowshaft of length l_a is assumed to be an inextensible Euler-Bernoulli beam hinged at the point of contact with the string by the nock. It is supported by the arrow rest and in the horizontal plane unilaterally guided by the pressure button with built-in spring with initial compression. At each end of the shaft there is a mass-point, the nock with mass m_{an} and the arrowhead with mass m_{at}. The cross-sectional quantities are the bending moment $M(\xi, t)$, a lateral force $V(\xi, t)$ in the ζ-direction and a longitudinal force $H(\xi, t)$ in the ξ-direction. The positive directions of M, V and H are shown in Figure 6.

In the coordinate system (ξ, ζ) the following set of PDE's describe the motion of the shaft of the arrow

$$\rho C \frac{\partial^2 \zeta}{\partial t^2}(\xi, t) = \frac{\partial V}{\partial \xi} \,, \tag{1}$$

$$V(\xi,t) = -\frac{\partial M}{\partial \xi} + H(\xi,t)\frac{\partial \zeta}{\partial \xi}\ , \tag{2}$$

$$M(\xi,t) = EI\frac{\partial^2 \zeta}{\partial \xi^2}\ , \tag{3}$$

where $\zeta(\xi,t)$ is the transverse deflection of the arrow which is a function of time t and distance ξ from the rear end. The circular cylindrical arrow is endowed with mass per unit of length ρC, where ρ is the specific mass of the shaft material, and with flexural rigidity EI, where E is Young's modulus of the shaft material. The area C of the material cross-section and its second moment of inertia I with respect to the centre-line of its cross-section are given by

$$C = \pi\left(d^2 - (d-2g)^2\right)/4 \ \text{ and } \ I = \pi\left(d^4 - (d-2g)^4\right)/64\ . \tag{4}$$

where d and g are the external diameter and the shaft wall thickness of the arrow, respectively, which are chosen to be independent of ξ. This holds for modern tubular arrowshafts. Formerly, solid wooden arrowshafts were used; in that case we have $g = 1/2d$. The total mass of the arrow is denoted by $2m_a = m_{an} + \rho C l_a + m_{at}$, where the factor 2 is inserted to account for symmetry of the bow. The longitudinal force $H(\xi,t)$, $0 < \xi < l_a$, along the arrow is coupled to the acceleration of the arrow in the x-direction. For $\xi \downarrow 0$ it is the acceleration force, $E(t) = -2m_a\ddot{b}$, exerted by the string on the arrow minus the force, $-m_{an}\ddot{b}$, needed to accelerate the nock. We assume that $E(t)$ is equal to the value found for the bow with the arrow treated as a point mass in the middle of the string, (Figure 4). For $\xi \in (0, l_a)$ the following expression holds

$$H(\xi,t) = \ddot{b}(t)\left(\rho C(l_a - \xi) + m_{at}\right)\ . \tag{5}$$

After arrow exit we have no acceleration force and because the arrow is inextensible $H(\xi,t) = 0$ for $t > t_l$.

We now give some considerations in connection with possible movements of the bow out of the (x,y)-plane during and after release. The movements are assumed to be small so that their influence is linear. The displacement of the grip in the z-direction is denoted by $g_G(t)$ and the angle of rotation around a line parallel to the y-axis and through the pivot point G on the x-axis, is denoted by $\alpha_{Gy}(t)$. Modern bows are often equipped with several stabilizers to reduce lateral movements as well as rotations of the bow. When shot by an individual archer from hand, experimental values of $g_G(t)$, measured as described in [10, 11], can be used to simulate the motion of the grip. Then the bow is held loosely by the archer so that it can rotate freely around the vertical axis through the pivot point G and equations of motion for the bow as a whole have to be formulated to determine $\alpha_{Gy}(t)$ in the course of the calculation of the motion of the arrow. When mechanical shooting machines are used, the grip is assumed to be at a fixed point in the coordinate system (x,y,z). In that case we have $g_G(t) = 0$ and also $\alpha_{Gy}(t) = 0$. All results presented in this paper hold for an arrow shot from a shooting machine and we take $h_g = 0$.

First we deal with the simple case in which the arrow is free from the pressure point, and we describe the boundary conditions for the set of PDE's, (1), (2) and (3) at $\xi = 0$ and $\xi = l_a$. One boundary condition for $\xi = 0$ is

$$M(0,t) = 0\ , \tag{6}$$

the bending moment being zero because the arrownock is assumed to be a point-mass and it rotates freely around the string. The other one follows for $0 \le t \le t_r$ from the movement of

the middle of the string during the time of release when the string slides over the finger tips, it is assumed to be

$$\zeta(0,t) = h_r \, \frac{|OD| - b(t)}{|OD| - b(t_r)} \, , \tag{7}$$

where t_r is the instant the string leaves the finger tips, $|OD| - b(t_r)$ the contact length and h_r the maximum displacement. The last two quantities depend on the archers technique and are assumed to be known. Thereafter ($t > t_r$) the motion of the rear end ($\xi = 0$) satisfies the equation of motion for the nock. In order to represent the transverse stiffness of the middle of the string, we introduce a spring of strength $k_z = \eta_z k_{zs}$, where k_{zs} is the measured static transverse elasticity of the bow and η_z is the associated efficiency. This spring tries to pull the nock back into the median plane of the bow. Then for $t_r < t < t_l$ the equation of motion reads (see also Figure 5)

$$\begin{aligned} &-m_{an}\frac{\partial^2\zeta}{\partial t^2}(0,t) - \frac{\partial M}{\partial \xi}(0,t) + H(0,t)\frac{\partial \zeta}{\partial \xi}(0,t) \\ &= k_z \left[\zeta(0,t) - \{g_G(t) + h_g - (b(t) + |OG|)\alpha_{Gy}(t)\}\right] \, , \end{aligned} \tag{8}$$

where we assume that $\alpha_{Gy}(t)$ is small. When the arrownock is free from the string, after arrow exit ($t > t_l$), we have $k_z = 0$. Observe that at arrow exit, the lateral force $V(0,t)$ can be discontinuous as a function of time at $t = t_l$. In that case the string jerks out of the nock.

The equations of motion for the mass of the arrowhead constitute the boundary conditions at $\xi = l_a$,

$$M(l_a, t) = 0 \, , \tag{9}$$

because the moment of inertia of the arrowhead is assumed to be zero, and

$$-\, m_{at}\frac{\partial^2\zeta}{\partial t^2}(l_a,t) + \frac{\partial M}{\partial \xi}(l_a,t) - H(l_a,t)\frac{\partial \zeta}{\partial \xi}(l_a,t) = 0 \, . \tag{10}$$

Next we deal with the case that the arrow slides along the bow and presses against the pressure point. The boundary conditions at $\xi = 0$ and $\xi = l_a$ remain the same as in the previous case. But now we have two sets of PDE's at the two adjacent intervals of the arrow connected at the position $\xi_\gamma(t)$ of the pressure point. This point of contact between the arrow and the pressure point moves in the (ξ, ζ)-coordinate system in the negative ξ-direction due to the forward motion of the arrow.

The longitudinal force $H(\xi, t)$ as well as the bending moment $M(\xi, t)$ are continuous with respect to ξ at $\xi_\gamma(t)$. However, the lateral force $V(\xi, t)$ shows a discontinuity at the pressure point. The jump in this force equals the contact force, denoted by $R(t) \geq 0$, exerted by the bow on the arrow, positive in the ζ-direction. It is given by

$$R(t) = \lim_{\xi \uparrow \xi_\gamma(t)} V(\xi,t) - \lim_{\xi \downarrow \xi_\gamma(t)} V(\xi,t) = -\lim_{\xi \uparrow \xi_\gamma(t)} \frac{\partial M}{\partial \xi}(\xi,t) + \lim_{\xi \downarrow \xi_\gamma(t)} \frac{\partial M}{\partial \xi}(\xi,t) \, , \tag{11}$$

where we used continuity of the force $H(\xi, t)$ and of the first derivative of $\zeta(\xi, t)$, both with respect to ξ at $\xi = \xi_\gamma(t)$. When a pressure button is used this force satisfies

$$R(t) = \begin{cases} 0 & , \ \zeta(\xi_\gamma(t),t) > g_G(t) + h_g, \\ \leq R_{g_{\min}} & , \ \zeta(\xi_\gamma(t),t) = g_G(t) + h_g, \\ R_{g_{\min}} + k_g(g_G(t) + h_g - \zeta(\xi_\gamma(t),t)), & \{\zeta(\xi_\gamma(t),t) \leq g_G(t) + h_g; \\ & \quad \zeta(\xi_\gamma(t),t) > g_G(t) + h_g - \epsilon\}, \\ \geq R_{g_{\max}}, & , \ \zeta(\xi_\gamma(t),t) = g_G(t) + h_g - \epsilon, \end{cases} \tag{12}$$

Table 1. Parameters and state variables; t=time, l=length, f=force, m=mass.

Parameters	Dimension	Interpretation
t	t	time
ξ	l	length coordinate along arrow
$\zeta(\xi,t)$	l	transverse deflection of arrow
$M(\xi,t)$	f l	bending moment in cross-section of arrow
$H(\xi,t)$	f l	longitudinal force in arrowshaft
l_a	l	length of arrow
m_{an}	m	mass of nock
m_{at}	m	mass of arrowhead
d	l	external diameter of arrowshaft
g	l	wall thickness of arrowshaft
C	l^2	area of cross-section of arrowshaft
I	l^4	moment of inertia of cross-section of arrowshaft
E	$f\,l^{-2}$	Young's modulus
ρ	ml^{-3}	mass density
$2m_a$	m	mass of arrow
k_{xs}	$f\,l^{-1}$	static longitudinal elasticity of bow
η_x	–	efficiency of bow
k_{zs}	$f\,l^{-1}$	static transverse elasticity of bow
η_z	–	efficiency of bow associated with transverse elasticity
h_r	l	maximum deflection of nock during release
h_g	l	protrusion of pressure point out of the median plane of bow
$g_G(t)$	l	transverse displacement of grip
$\alpha_{Gy}(t)$	–	angle of rotation of bow
k_g	$f\,l^{-1}$	spring constant of pressure button
$R(t)$	f	contact force at pressure point
t_r	t	instant string leaves finger tips
t_f	t	instant arrow becomes free from pressure point
t_l	t	instant arrow leaves string
t_g	t	instant nock passes pressure point

where we introduced k_g, $R_{g_{\min}}$, ϵ and $R_{g_{\max}}$ which characterize the pressure button. First, k_g is the spring constant of the spring of the pressure button. Second, $R_{g_{\min}}$ is caused by the initial compression of the spring, hence for $R \leq R_{g_{\min}}$ the pressure point does not move towards the grip. Third, ϵ is the maximum length over which the pressure point can move towards the grip. Fourth, $R_{g_{\max}}$ is the smallest number for which, when $R \geq R_{g_{\max}}$, the pressure point has approached the grip by ϵ.

The initial conditions, which complete the formulation of the problem, are

$$\zeta(\xi,0) = \frac{h_g}{|GD|}\,\xi \quad \text{and} \quad \frac{\partial \zeta}{\partial t}(\xi,0) = 0\,, \tag{13}$$

hence at $t = 0$, the arrow is straight, but does not have to lie along the line of symmetry of the bow.

Observe that the set of PDE's (1), (2) and (3) is linear, however, the contact-condition (12) is nonlinear. In a strict sense the non-homogeneous boundary conditions (7) and (8) also

make the problem nonlinear with respect to a superposition of solutions for different initial conditions (13).

Generally in problems with moving boundaries, the position of the boundary is unknown and has to be determined. In our case, as we mentioned in the introduction, the position of the boundary between the two parts of the arrow is known in advance, its distance to the end of the arrow equals $\xi_\gamma(t) = b(t) + |OG|$.

We calculate also the total acceleration force acting on the arrow in the ζ-direction. This quantity is calculated twice. First, $F_{tot}(t)$ as the integral over the mass distribution times the local acceleration in the ζ-direction,

$$F_{tot}(t) = \int_0^{l_a} \rho \frac{\partial^2 \zeta}{\partial t^2}(\xi, t)\, \mathrm{d}\xi + m_{an} \frac{\partial^2 \zeta}{\partial t^2}(0, t) + m_{at} \frac{\partial^2 \zeta}{\partial t^2}(l_a, t)\ . \tag{14}$$

Second, $F^+_{tot}(t)$ as the sum of the contact force $R(t)$ and the force $k_z \zeta(0, t)$ representing the transverse stiffness of the bow.

$$F^+_{tot}(t) = R(t) - k_z \zeta(0, t)\ . \tag{15}$$

For $t \geq t_r$ we have $F_{tot} = F^+_{tot}$. For the short time interval $0 \leq t \leq t_r$ we have $F^+_{tot} \neq F_{tot}$. In that case the transverse force $L(t)$ exerted by the archers fingers and associated with the prescribed displacement of the nock, is the difference between the two expressions (14) and (15), $L(t) = F_{tot} - F^+_{tot}$.

3. Finite-difference equations

In the finite-difference method, discretizations are taken for both the spatial and temporal coordinates. The region to be examined is covered by a rectilinear grid with sides parallel to the ξ- and t-axes, with $\Delta\xi$ and Δt being the grid spacing in the ξ- and t-directions, respectively. The grid points (ξ, t) are given by $\xi = i\,\Delta\xi$ and $t = j\,\Delta t$, where i and j are integers and $i = j = 0$ is the origin. In each grid point there are two state variables, namely the displacement ζ and the bending moment M. The domain of i is $-1 \leq i \leq n + 1$ where $n\,\Delta\xi = l_a$ and $j = 0(1)m$ where m is large enough to cover the time interval of interest. We use the following notation for the deflection $\zeta^j_i = \zeta(i\Delta\xi, j\Delta t)$ and for the bending moment $M^j_i = M(i\Delta\xi, j\Delta t)$. By substitution of V from (2) in (1) we eliminate V. Then with (3) we have two equations for the two unknowns ζ and M, namely

$$\rho C \frac{\partial^2 \zeta}{\partial t^2}(\xi, t) = -\frac{\partial^2 M}{\partial \xi^2} + \frac{\partial H(\xi, t)}{\partial \xi} \frac{\partial \zeta}{\partial \xi} + H(\xi, t) \frac{\partial^2 \zeta}{\partial \xi^2}\ , \tag{16}$$

$$M(\xi, t) = EI \frac{\partial^2 \zeta}{\partial \xi^2}\ . \tag{17}$$

We keep M as one of the unknowns because then the boundary conditions can be implemented easier. The fictitious points outside the range of the arrow are introduced to get a higher-order approximation of these boundary conditions at the nock and arrowhead.

The implicit finite-difference formulas for (16) and (17) are, see also [6], with $0 \leq i \leq n$

$$\rho C\, \frac{\zeta^{j+1}_i - 2\zeta^j_i + \zeta^{j-1}_i}{(\Delta t)^2} =$$

$$\mu\left(-\frac{M_{i+1}^{j+1}-2M_i^{j+1}+M_{i-1}^{j+1}}{(\Delta\xi)^2}+\frac{\partial H(i\Delta\xi,(j+1)\Delta t)}{\partial\xi}\frac{(\zeta_{i+1}^{j+1}-\zeta_{i-1}^{j+1})}{2\Delta\xi}+\frac{M_i^{j+1}}{EI}\right)+$$
$$(1-\mu)\left(-\frac{M_{i+1}^{j-1}-2M_i^{j-1}+M_{i-1}^{j-1}}{(\Delta\xi)^2}+\frac{\partial H(i\Delta\xi,(j-1)\Delta t)}{\partial\xi}\frac{(\zeta_{i+1}^{j-1}-\zeta_{i-1}^{j-1})}{2\Delta\xi}+\frac{M_i^{j-1}}{EI}\right)\,, \tag{18}$$

$$M_i^{j+1}=EI\,\frac{\zeta_{i+1}^{j+1}-2\zeta_i^{j+1}+\zeta_{i-1}^{j+1}}{(\Delta\xi)^2} \tag{19}$$

where μ is a coefficient; when $\mu=1$ the scheme is the first-order backward Euler scheme and when $\mu=\frac{1}{2}$ it is the second-order Crank-Nicolson scheme. The boundary conditions (6), (7) and (8) for $\xi=0$ and (9) and (10) for $\xi=l_a$, are discretized by similar schemes.

The initial conditions (13) become

$$\zeta_i^0=\frac{h_g}{|GD|}\,i\Delta\xi\ \text{ and }\ \zeta_i^1-\zeta_i^{-1}=0\,. \tag{20}$$

The latter equation is used to eliminate ζ_i^{-1} from (18) for $j=0$ with $\mu=1$.

We now discuss the discretization of the contact condition (12) at the pressure point, where, as we mentioned before, the third-order spatial derivative of the deflections ζ will show a discontinuity. We deal with (16) together with (17) on each of the adjacent intervals $(0,\xi_\gamma)$ and (ξ_γ,l_a). The solutions of (16) and (17) are coupled by (12) while, ζ, $\frac{\partial\zeta}{\partial\xi}$ and $\frac{\partial^2\zeta}{\partial\xi^2}$ (hence also M) are continuous at $\xi=\xi_\gamma$. We define g as annteger, so that $\xi_\gamma\in[g\Delta\xi,(g+1)\Delta\xi]$. As for the boundary conditions at $\xi=0$ and $\xi=l_a$ we introduce fictitious points outside the ranges $[0,\xi_\gamma]$ and $[\xi_\gamma,l_a]$ so that we have two extra grid points for g, and $g+1$. However, continuity of the transverse displacements together with the first and second-order partial derivatives implies that the two transverse displacements in the associated real and fictitious point are equal. Hence, we do not have to introduce these fictitious points explicitly with respect to the displacement, but we used the three continuity conditions implicitly. The displacement at point ξ_γ is obtained by interpolation with a cubic spline in the interval $[\xi_g,\xi_{g+1}]=[g\Delta\xi,(g+1)\Delta\xi]$.

In order to be able to approximate (11) more appropriately, we kept the two fictitious points for the bending moment; one in point $g\Delta\xi$ where this bending moment is denoted by M_+, and the other in point $(g+1)\Delta\xi$ with bending moment M_- (Figure 6). As a result, in (18) for $i=g$ the bending moment M_{g+1} has to be replaced by M_- and for $i=g+1$, M_g by M_+. Equation (11) for $R(t)$ is decretisized by

$$R((j+1)\Delta t)=\frac{-M_-^{j+1}+M_g^{j+1}+M_{g+1}^{j+1}-M_+^{j+1}}{\Delta\xi} \tag{21}$$

and (12) by

$$R((j+1)\Delta t)=\begin{cases}0 & ,\ \zeta_g^{j+1}\geq g_G((j+1)\Delta t)+h_g\,,\\ \leq R_{g_{\min}} & ,\ \zeta_g^{j+1}=g_G((j+1)\Delta t)+h_g\,,\\ R_{g_{\min}}+k_g\{g_G((j+1)\Delta t)+h_g-\zeta_g^{j+1}\} & ,\ \{\zeta_g^{j+1}\leq g_G((j+1)\Delta t)+h_g\,,\\ & \quad \zeta_g^{j+1}>g_G((j+1)\Delta t)+h_g-\epsilon\}\,,\\ \geq R_{g_{\max}} & ,\ \zeta_g^{j+1}=g_G((j+1)\Delta t)+h_g-\epsilon\,.\end{cases} \tag{22}$$

To avoid numerical problems associated with the collision and rebound when the arrow makes contact with the pressure point, we introduce a large spring constant k_g^* (possibly the elasticity of the plastic end piece of the small rod of the pressure button) for the two inflexible positions of the unilateral support.

At each time step we have to solve a set of linear equations. Initially we assume that in the considered time step, $j\Delta t \leq t \leq (j+1)\Delta t$, the arrow does not switch its state of contact with the pressure point. If there was contact and the resulting contact force is negative, $R((j+1)\Delta t) < 0$, or the arrow was free from the pressure point and the deflection of the arrow at the position of the pressure point is smaller than the displacement of the pressure point itself, $\zeta(\xi_\gamma(t), t) < g_G(t) + h_g$, (Equation (12)), then the calculations are repeated with the arrow free from the pressure point, or in contact with the pressure point, respectively.

A combination of the backward-Euler and the Crank-Nicolson technique is used. For the first time step ($j = 0$), when the point of contact moves in the time step into the adjacent interval ($g((j+1)\Delta t) \neq g(j\Delta t)$) and, in addition, when in the considered time step the state of contact between arrow and pressure point changes, we used the robust backward-Euler scheme, $\mu = 1$. Otherwise we used the more accurate Crank-Nicolson scheme, $\mu = \frac{1}{2}$.

This finite-difference scheme is used to get the results presented in the next sections. To evaluate the performance of the finite-difference scheme we studied first a vibrating beam hinged at both ends. Because this allows closed-form solutions, we are able to compare this solution with the numerical solution, thus obtaining insight into effective values for $\Delta\xi$ and Δt. All results presented were obtained with $n = 32$ and $\Delta t = 0 \cdot 01$ ms.

4. Results and discussion

Pękalski defines the concept ‘standard bow and arrow’. This is the equipment used by one of the best Polish archery competitors. Table 2 gives under the headings “both models” and “Pękalski’s model” a survey of all parameters of this standard bow and arrow, taken from [4].

In Figure 7 we give the shapes calculated by Pękalski of the standard arrow shot with the standard bow for every 2 milliseconds (ms) after release. Note that here, as in Figure 8, the transverse motion ζ is given as a function of x and t instead of as a function of ξ and t. Also, the experimental shapes are shown. Pękalski estimated three parameters, (two of these are $\eta_x = 0 \cdot 76$ and $\eta_z = 0 \cdot 71$), used in his theory, by a least-squares fit of the calculated results with the experimental data.

In our model we used the parameters provided by Pękalski in [4], except those given in Table 2 under the heading “this model”, which we discuss briefly in the following.

We used the DFD curve shown in Figure 4 which belongs to the Greenhorn Comet TD 350, 68 inch, 30 lbs. This bow differs slightly from the Hoyt Pro Medalist T/D, 66 inch, 34 lbs bow, used by Pękalski.

The flexural rigidity of the arrow $EI = 2 \cdot 088\text{Nm}^2$ used by Pękalski (Table 2) is smaller than the value supplied by the manufacturer of the arrow. We used the value supplied by the manufacturer namely $EI = 0 \cdot 0037\ 10^{-8} \times 7 \cdot 1\ 10^{10} = 2 \cdot 6\ \text{Nm}^2$. Also the masses of both arrows differ slightly. In [9] the mass of the Easton 1616X75 is $0 \cdot 0183$ kg while the mass of the 1714X7 arrow Pękalski used is $0 \cdot 0188$ kg. Therefore some small scaling adjustments to $E(t)$ being the DFD curve shown in Figure 4, had to be made. The weight of our bow is not taken equal to the weight of the bow modeled as a linear spring by Pękalski, but is chosen so that the amount of available energy in the drawn bow $\int_{|OH|}^{|OD|} F(b)\,\mathrm{d}b$ is the same as that in the

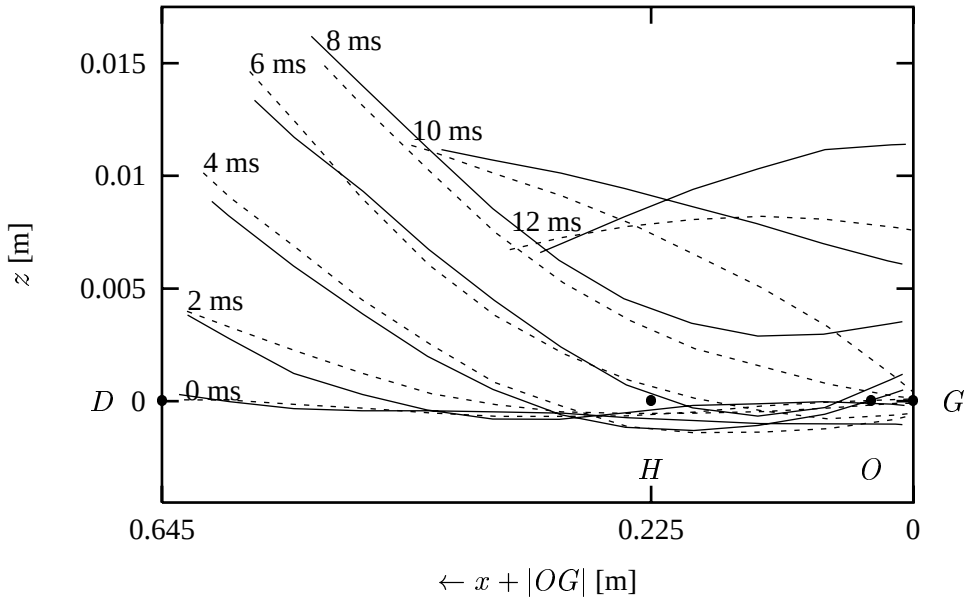

Figure 7. Deformation of arrow: experimental data (- - -) and calculated by Pękalski (——), every 2 ms after release, [5]. Only parts of the arrow for $\xi \in [0, \xi_\gamma(t)]$ are shown.

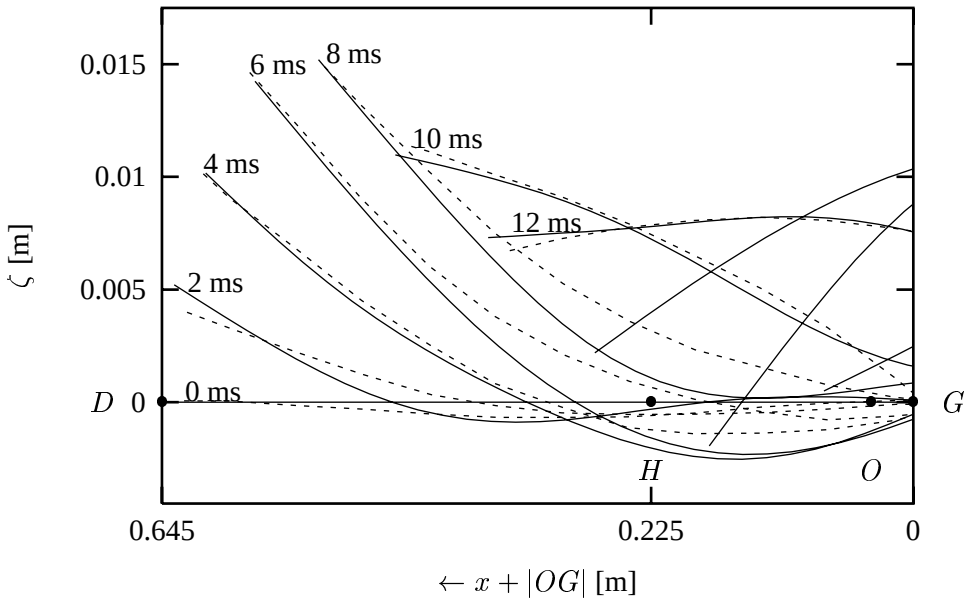

Figure 8. Deformation of arrow: experimental data (- - -) after Pękalski [5], on basis of model derived in this paper (——), every 2 ms after release, until arrow nock passes pressure point at $t = t_g$. Only parts of the arrow for $\xi \in [0, \xi_\gamma(t)]$ are shown.

linear spring model with spring stiffness k_{xs}, $1/2 k_{xs}(|OD| - |OH|)^2$, while the efficiency is taken equal to the value estimated by Pękalski; $\eta_x = 0 \cdot 76$.

For the pressure button we used the following measured quantities of an OK button, $k_g = 622$ N/m, $R_{g_{min}} = 3 \cdot 3$ N, $R_{g_{max}} = 7 \cdot 65$ N, hence $\epsilon = 0 \cdot 007$ m. The elasticity of the

Table 2. Values for the parameters of the Easton 1714X7 (Aluminum 7178) arrow after [4]. The bow is a Hoyt Pro Medalist T/D, 66 inch, 34 lbs. For the standard arrow-bow combination Pękalski estimated: $\eta_x = 0 \cdot 76$, $\eta_z = 0 \cdot 71$.

parameter	unit	1714X7	parameter	unit	1714X7
both models					
d	m	0·00675	g	m	0·000356
C	m^2	$0{\cdot}0723\ 10^{-4}$	ρ	kg m^{-3}	$2{\cdot}82\ 10^3$
l_a	m	0·67	$2m_a$	kg	0·0188
m_{an}	kg	0·0014	m_{at}	kg	0·004
$\|OD\|$	m	0·584	$\|OH\|$	m	0·164
$\|GD\|$	m	0·645	$\|GH\|$	m	0·225
η_x	–	0·76	k_{zs}	N/m	270
Pękalski's model					
k_{xs}	N/m	342	η_z	–	0·71
$F(\|OD\|)$	N	143	EI	Nm^2	2·088
this model					
$\|OD\| - b(t_r)$	m	0·0035	h_r	m	0·00229
$F(\|OD\|)$	N	119	EI	Nm^2	2·6
h_g	m	0	η_z	–	0·68
k_g	N/m	622	k_g^*	N/m	18000

plastic end piece of the button is taken equal to $k_g^* = 18000$ N/m. In Equation (7) we have taken $|OD| - b(t_r) = 0 \cdot 0035$ m. The parameter h_r is equal to $0 \cdot 00229$ m, the efficiency η_z equals $0 \cdot 68$ and both are tuned so that a good fit is obtained with the experimental data presented in [4, 5]. We used in all cases $h_g = 0$ (centre-shot bow).

In Figure 8 the shapes of the arrow obtained by means of our model, are compared with experimental shapes obtained by Pękalski. The arrow undergoes a series of bends before its nock passes the grip. The first bend is with both the arrowhead and especially the nock moving to the left (from the point of view of the right-handed archer) while the middle of the arrow moves to the right. After that the arrow oscillates and its frequency is retarded by the normal force in the shaft of the arrow. As the string approaches brace height, $t \approx 0 \cdot 015$ s, the nock is to the right of the median plane. This is caused by the transverse elasticity of the bow which tries to pull the nock back into the median plane. At this time the arrowshaft is bending exactly opposite to the first mentioned bend. As the bow string moves beyond the brace height, the arrow flexes a third time, in a manner similar to the first bend. This is favorable, since it helps the fletching to clear the bow. The whole sequence allows the arrow to snake around the pressure point; see Figure 8 in which also the calculated shapes for t =14, 16 and 18 ms are partly shown.

In Figure 9 the contact force $R(t)$ as a function of time t is shown. Shortly after release at $t = t_r$ there is contact between the arrow and the pressure point, but the contact force is small and the arrow looses contact quickly. Thereafter the arrow touches once more the pressure point and there is a longer period in which there is contact with the pressure point whereby $R(t)$ is much larger. After $t = t_f$ the arrow is definitively free from the pressure point, but the arrow is still accelerated by the string.

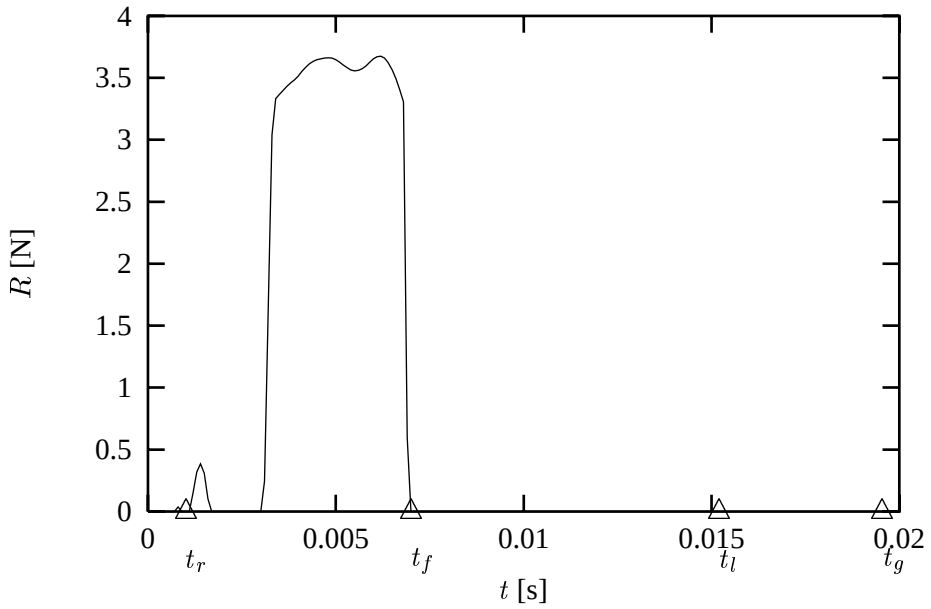

Figure 9. Contact force $R(t)$. (——) obtained by means of acceleration force $E(b)$ of Figure 4. Arrow leaves pressure point definitely at $t = t_f$. Arrow leaves string at $t = t_l$ and nock passes pressure point at $t = t_g$.

Figure 10 gives the total force in the ζ-direction acting on the arrow. The difference between the two curves F_{tot} and F_{tot}^{+} for $t \geq t_r$, which must be zero, is small; this is a check on the implementation of the equations in the computer code. For $t \leq t_r$ this difference is the transverse force applied by the finger tips upon the string during release. Observe that this force is rather large for the first time step $j = 1, t = \Delta\xi$. This is due to the discontinuity of the velocity $\frac{\partial\zeta}{\partial t}(0,0)$ of the nock in the ζ-direction at $t = 0$; analytically this force has to be a Dirac delta function. If the enforced displacement function given by (7) were quadratic instead of linear, this discontinuity would disappear. Fortunately, calculations showed that the motion after release is not very sensitive with respect to the precise shape of this function, but depends on the increase of momentum in the ζ-direction during release.

When the acceleration force becomes zero at $t = t_l$, the arrow leaves the string. Observe that the discontinuity of the transverse force on the nock in $t = t_l$ is rather small and this suggests a rather smooth separation of string and arrownock. For $t \geq t_l$ the arrow continues to oscillate as a free-free beam with (rather small) point masses m_{at} and m_{an} at the fore and the rear ends, respectively. For $t = t_g$ the nock of the arrow passes the grip of the bow after which the still vibrating arrow is on its way to the target.

In Figure 11 is shown the sum of the transverse kinetic energy of the arrow and the potential energies of the arrow, of the spring which represents the transverse elasticity of the bow and of the spring in the pressure button, as a function of time.

For $0 \leq t \leq t_r$ transverse energy is gained from the bow by means of the way of releasing. For $t \geq t_r$ the transverse energy can be fed by the force $H(\xi, t)$ and therefore by $E(b)$. We observe that the maximum amount of transverse energy in the arrow (0·05 Nm) is small with respect to the available amount of energy in the fully drawn bow (30·2 Nm) and this justifies the use of the decoupling of the transverse motion of the arrow from its longitudinal motion. After $t \geq t_l$ we have $H(\xi, t) = 0$ and the transverse energy is almost constant.

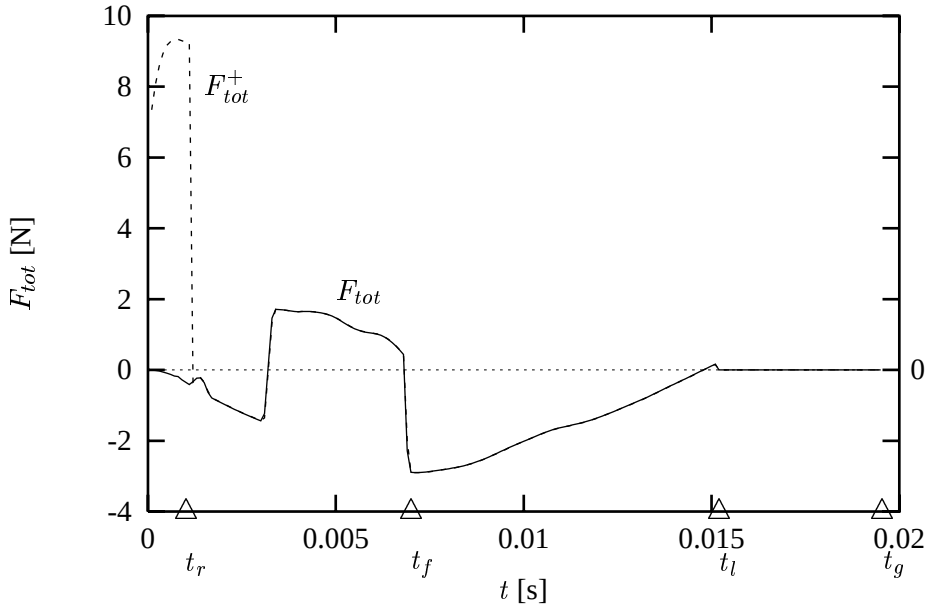

Figure 10. Total force F_{tot} acting on arrow in ζ-direction (14), (– –). Also F_{tot}^+, (15), (——), is shown. $F_{tot}^+ = F_{tot}$ for $t > t_r$. Arrow looses contact with pressure point definitely at $t = t_f$. Arrow leaves string at $t = t_l$ and nock passes pressure point at $t = t_g$.

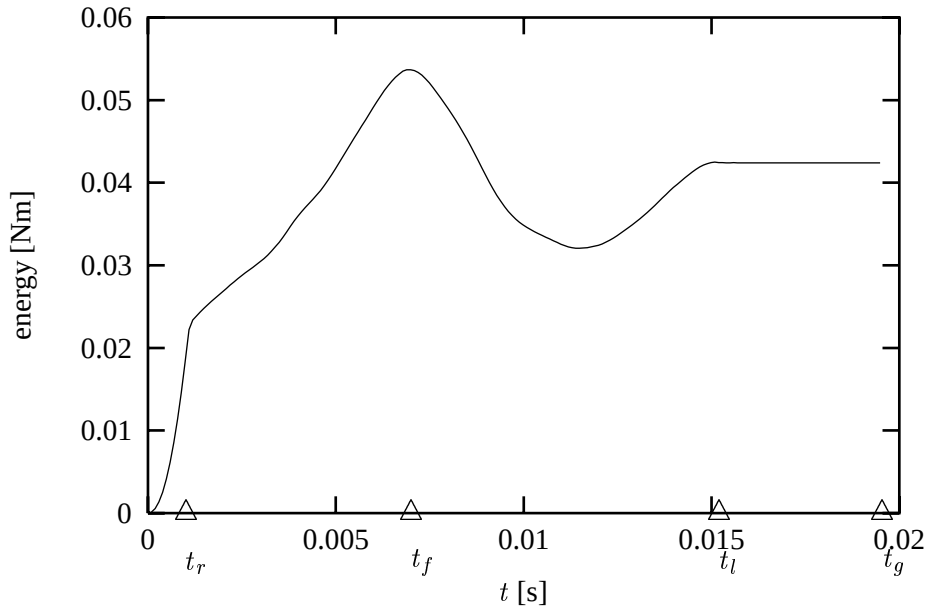

Figure 11. Transverse kinetic energy plus potential bending energy of arrow plus energy in spring which represents transverse elasticity of bow plus energy in spring of pressure button.

We performed a sensitivity analysis with respect to the external diameter of the arrowshaft, d. For the standard arrow we have $d = 17/64$ inch. Two other diameters are considered, namely a more flexible arrow with $d = 15/64$ inch and a stiffer arrow $d = 21/64$ inch, where the shaft wall thickness $g = 14/1000$ inch for each of the three arrows. Observe that the mass

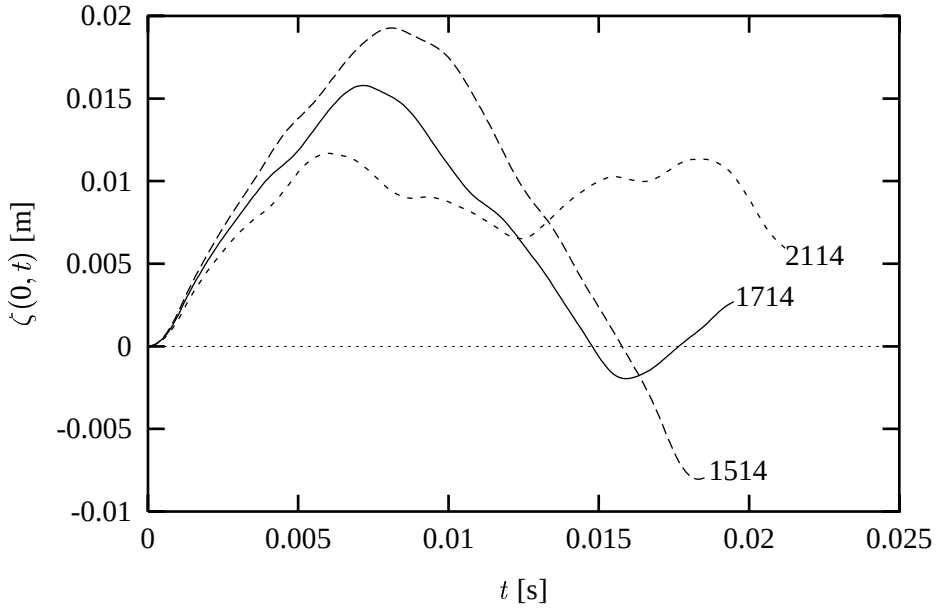

Figure 12. Paths of nock of three different arrows until nock passes pressure point. (——) standard arrow 1714X7, (– –) stiffer (and heavier) arrow 2114X7 and (- - -) more flexible (and lighter) arrow 1514X7. Latter arrow slaps against pressure point.

of the arrow changes simultaneously, for instance the more flexible arrow is also lighter. In Figure 12 the paths of the nocks of the three arrows are compared, until they pass the pressure point. The more flexible arrow slaps against the pressure point. This is undesirable. The stiffer arrow clears the grip in a more pronounced fashion, but this results in a rather large jump in the transverse force at the nock of the arrow when it leaves the string. The reason is that this force is proportional to the deflection of the nock at that moment.

Pękalski's model predicts for the standard arrow, $d = 17/64$ inch, that the displacement of the nock of the arrow out of the median plane is zero for a relatively long time interval preceding arrow exit at $t = t_l$. His calculations for soft $d = 15/64$ inch and stiff $d = 21/64$ inch arrows suggest that there was not such a period for these two arrows. On the basis of these results Pękalski formulated the following definition of a well-selected bow-arrow combination:

> A well-selected bow-arrow subsystem is any system for which the dimensionless parameters of the mathematical model of the arrow's movement during its contact with the bow have the same values as for the 'standard' system.

Pękalski introduced dimensionless variables and parameters using l_a, $\sqrt{l_a^{-4}\, EI/\rho C}$ and l_a^3/EI for length, time and length per force, respectively. Ths, his definition attempts to formulate in words that the jump in the transverse force acting upon the nock at arrow exit is small for a well-chosen arrow. Our results, however, show that even for the standard arrow no long time period preceding arrow exit exists where the displacement of the nock is small. In our model the arrow leaves the string at the instant the nock passes the median plane again (Figure 12). Hence, the definition of Pękalski of a well-selected bow-arrow combination may still be useful, although it cannot be based on the stay of the nock of the arrow for a long period of time in the neighborhood of the median plane of the bow.

5. Conclusions

Due to the inertia of the bow limbs the SFD and the DFD curves differ significantly. Figure 4 gives the calculated SFD and the DFD curves for a modern working-recurve bow.

In the literature two phenomena are mentioned in explaining the 'Archers Paradox': first, the vibration of the arrow as a vibrating beam; second, the distributed buckling force due to the acceleration force acting upon the rear end of the arrow, which is enlarged by the arrowhead. The results obtained in this paper show that the transverse forces associated with the release, as well as the transverse flexibility of the bow and the contact force exerted by the pressure point are important. The oscillatory motion is started by the enforced displacement of the nock during release.

The numerical results obtained fit the experimental data from a high-speed film well, at least as well as those of Pękalski's model. Observe that the shapes of the arrow for $t = 10$ and $t = 12$ ms predicted by our model (Figure 8), are better than those predicted with Pękalski's model as shown in Figure 7. It is seen that also a better description is obtained for the important time period between the detachment of the nock from the string until it passes the pressure point. Our model makes use of experimental evidence, such as the motion of the string as it comes off the drawing fingers, and is more consistent and detailed than Pękalski's model. This makes it possible to investigate in the future more subtle effects, such as the influence of different arrow dimensions, stabilizers, brace heights, and types of release and of the influence of the grip of individual competition archers on the bow.

Acknowledgements

The first author wishes to acknowledge the help of Prof. R. Grucza and Dr. K. Kedzior of the Institute of Sport, Warshaw, Poland. He thanks Dr. Pękalski for valuable information and Pim Pouw for the measurement of the characteristics of his pressure button.

References

1. C. N. Hickman, F. Nagler, and P. E. Klopsteg. *Archery: the technical side*. Redland (CA): National Field Archery Association (1947) 281pp.
2. R. Hardy. *Longbow*. Sparkford (Somerset, UK): Patrick Stephens Limited (1992) 244pp.
3. W. F. Paterson. A "Mary Rose" archery symposium. *Journal of the Society of Archer-Antiquaries* 26 (1983) 49-51.
4. R. Pękalski. *Modelling and simulation research of the competitor-bow-arrow system (in Polish)*. PhD thesis, Academy of Physical Education, Warsaw (1987) 122pp.
5. R. Pękalski. Experimental and theoretical research in archery. *Journal of Sports Sciences* 8 (1990) 259-279.
6. B. W. Kooi. *On the Mechanics of the Bow and Arrow*. PhD thesis, Rijksuniversiteit Groningen (1983) 211pp.
7. B. W. Kooi and J. A. Sparenberg. On the static deformation of a bow. *Journal of Engineering Mathematics* 14 (1980) 27-45.
8. B. W. Kooi. On the mechanics of the bow and arrow. *Journal of Engineering Mathematics* 15 (1981) 119-145.
9. B. W. Kooi. On the mechanics of the modern working-recurve bow. *Computational Mechanics* 8 (1991) 291-304.
10. C. Gallozzi, L. M. Leonardi, A. Pace, and G. Caselli. A new method to measure lateral bow accelerations during shooting in archery. In: G. Bergmann, R. Kölbel, and A. Rohlmann (eds.), *Biomechanics: Basic and Applied Research* (1987) pp. 639-644.
11. L. M. Leonardi, C. Gallozzi, A. Pace, and A. Dal Monte. Reduction of lateral bow displacement using different torque flight compensators and stabilizers in archery. In: G. Bergmann, R. Kölbel, and A. Rohlmann, editors, *Biomechanics: Basic and Applied Research* (1987) pp. 633-638.